



Hot-Pressed versus Sintered $\text{LiTi}_2(\text{PO}_4)_3$

by Jeff Wolfenstine, Jan L. Allen, and James Sumner

ARL-TR-4716

February 2009

NOTICES

Disclaimers

The findings in this report are not to be construed as an official Department of the Army position unless so designated by other authorized documents.

Citation of manufacturer's or trade names does not constitute an official endorsement or approval of the use thereof.

Destroy this report when it is no longer needed. Do not return it to the originator.

Army Research Laboratory

Adelphi, MD 20783-1197

ARL-TR-4716

February 2009

Hot-Pressed versus Sintered $\text{LiTi}_2(\text{PO}_4)_3$

Jeff Wolfenstine, Jan L. Allen, and James Sumner
Sensors and Electron Devices Directorate, ARL

REPORT DOCUMENTATION PAGE

Form Approved
OMB No. 0704-0188

Public reporting burden for this collection of information is estimated to average 1 hour per response, including the time for reviewing instructions, searching existing data sources, gathering and maintaining the data needed, and completing and reviewing the collection information. Send comments regarding this burden estimate or any other aspect of this collection of information, including suggestions for reducing the burden, to Department of Defense, Washington Headquarters Services, Directorate for Information Operations and Reports (0704-0188), 1215 Jefferson Davis Highway, Suite 1204, Arlington, VA 22202-4302. Respondents should be aware that notwithstanding any other provision of law, no person shall be subject to any penalty for failing to comply with a collection of information if it does not display a currently valid OMB control number.

PLEASE DO NOT RETURN YOUR FORM TO THE ABOVE ADDRESS.

1. REPORT DATE (DD-MM-YYYY) February 2009		2. REPORT TYPE Interim		3. DATES COVERED (From - To)	
4. TITLE AND SUBTITLE Hot-Pressed versus Sintered LiTi ₂ (PO ₄) ₃				5a. CONTRACT NUMBER	
				5b. GRANT NUMBER	
				5c. PROGRAM ELEMENT NUMBER	
6. AUTHOR(S) Jeff Wolfenstine, Jan L. Allen, and James Sumner				5d. PROJECT NUMBER	
				5e. TASK NUMBER	
				5f. WORK UNIT NUMBER	
7. PERFORMING ORGANIZATION NAME(S) AND ADDRESS(ES) U.S. Army Research Laboratory ATTN: AMSRD-ARL-SE-DC 2800 Powder Mill Road Adelphi, MD 20783-1197				8. PERFORMING ORGANIZATION REPORT NUMBER ARL-TR-4716	
9. SPONSORING/MONITORING AGENCY NAME(S) AND ADDRESS(ES)				10. SPONSOR/MONITOR'S ACRONYM(S)	
				11. SPONSOR/MONITOR'S REPORT NUMBER(S)	
12. DISTRIBUTION/AVAILABILITY STATEMENT Approved for public release; distribution unlimited.					
13. SUPPLEMENTARY NOTES					
14. ABSTRACT The electrical and mechanical properties of hot-pressed versus sintered LiTi ₂ (PO ₄) ₃ were investigated. The hot-pressed LiTi ₂ (PO ₄) ₃ had a higher density and larger average grain size than the sintered material. As a result of these microstructural differences, the hot-pressed material exhibited a higher total ionic conductivity and lower hardness. The electronic conductivity of both materials was the same, and increased by a factor of about 10 ⁷ when the hot-pressed and sintered materials were heated under a reducing atmosphere.					
15. SUBJECT TERMS LiTi ₂ (PO ₄) ₃ , sintering, hot-pressing, ionic conductivity, electronic conductivity, hardness, microstructure					
16. SECURITY CLASSIFICATION OF:			17. LIMITATION OF ABSTRACT UU	18. NUMBER OF PAGES 28	19a. NAME OF RESPONSIBLE PERSON Jeff Wolfenstine
a. REPORT U	b. ABSTRACT U	c. THIS PAGE U			19b. TELEPHONE NUMBER (Include area code) 301-394-0317

Contents

List of Figures	iv
Acknowledgments	v
1. Introduction	1
2. Experimental	2
2.1 Powder Characterization	2
2.2 Consolidation.....	2
2.3 Property Characterization.....	2
3. Results and Discussion	3
3.1 Color.....	3
3.2 Particle Size.....	3
3.3 Structure	4
3.4 Differential Thermal Analysis.....	5
3.5 Density.....	6
3.6 Microstructure	7
3.7 Electronic Conductivity.....	9
3.8 Ionic Conductivity.....	10
3.9 Electronic Conductivity Under Reducing Atmosphere.....	12
3.10 Microhardness	14
4. Conclusions	15
5. References	16
Distribution List	19

List of Figures

Figure 1. Scanning electron micrograph of the initial $\text{LiTi}_2(\text{PO}_4)_3$ powders.	4
Figure 2. (a) X-ray diffraction pattern of the as-received $\text{LiTi}_2(\text{PO}_4)_3$ powders, (b) X-ray diffraction pattern of the $\text{LiTi}_2(\text{PO}_4)_3$ powders after sintering, (c) X-ray diffraction pattern of the $\text{LiTi}_2(\text{PO}_4)_3$ powders after hot-pressing, and (d) X-ray diffraction pattern of the $\text{LiTi}_2(\text{PO}_4)_3$ powders after hot-pressing and annealing.....	5
Figure 3. Differential thermal analysis curve (heating) for $\text{LiTi}_2(\text{PO}_4)_3$ powders.	6
Figure 4. Scanning electron micrograph of sintered $\text{LiTi}_2(\text{PO}_4)_3$ fracture surface.	8
Figure 5. Scanning electron micrograph of hot-pressed $\text{LiTi}_2(\text{PO}_4)_3$ fracture surface.	8
Figure 6. Scanning electron micrograph of hot-pressed and annealed $\text{LiTi}_2(\text{PO}_4)_3$ fracture surface.	9
Figure 7. Complex impedance plot of sintered and hot-pressed and annealed $\text{LiTi}_2(\text{PO}_4)_3$	10
Figure 8. High frequency region of the complex impedance plot of sintered and hot-pressed and annealed $\text{LiTi}_2(\text{PO}_4)_3$	11
Figure 9. X-ray diffraction pattern of the $\text{LiTi}_2(\text{PO}_4)_3$ sintered sample after heating under a reducing atmosphere.	13
Figure 10. X-ray diffraction pattern of the $\text{LiTi}_2(\text{PO}_4)_3$ hot-pressed and annealed sample after heating under a reducing atmosphere.	14

Acknowledgments

The authors would like to acknowledge support of the U. S. Army Research Laboratory (ARL), and Dr. Ivan Lee (ARL) for his help in performing the surface area measurements. In addition, the authors would like to acknowledge the help of Dr. William Luecke of the National Institute of Standards and Technology for his help in performing the microhardness measurements.

INTENTIONALLY LEFT BLANK.

1. Introduction

Recently, there has been a renewed interest in the development of high energy Lithium (Li)-Air batteries. One configuration involves the use of a Li anode in a non-aqueous electrolyte, which is separated from an aqueous electrolyte containing the air cathode by a solid state Li-ion conducting membrane (1). One material under consideration for use as a membrane is $\text{LiTi}_2(\text{PO}_4)_3$ (LTP). LTP meets the material requirements of high Li-ion lattice conductivity and chemical stability with the electrolytes (2–7). A processing requirement for the LTP membrane is very high density. Very high density is important for several reasons. Firstly, it has been observed for LTP that the total Li-ion conductivity (lattice plus grain boundary) is a strong function of density. For example, Li-ion conductivity can vary from about 2×10^{-9} S/cm (8) for a material with a relative density (actual density/theoretical density) around 70% to about 1×10^{-3} S/cm for a material with a relative density close to 100% (8–11). It has been suggested that high density is required to reduce grain boundary resistance (7). Secondly, a high density is required for safety, so that no water ever comes in contact with the Li anode. Thirdly, mechanical strength is known to increase with increasing density (12–14). In order to achieve high density LTP, two processing approaches are commonly used. The first approach is to melt doped-LTP, followed by quenching, to form a glass which is subsequently reheated to allow for the formation of a glass-ceramic (9,10). The second approach is to use conventional sintering of LTP, but dope it with a trivalent impurity (i.e., Al^{+3}) on the Ti site and extra Li (charge compensation for Al^{+3} on the Ti^{+4} site), or to add a low melting boundary phase (2–8). These methods must be used because it has been observed that pure $\text{LiTi}_2(\text{PO}_4)_3$ cannot be sintered to high densities (2–8,11). Another possible processing method to obtain high density pure LTP is to use hot-pressing. In this case, the applied stress adds an additional driving force for densification compared to conventional sintering, hence, a higher density should be obtainable over conventional sintering, therefore resulting in improved electrical and mechanical properties (12–14).

The only one brief study on hot-pressed LTP (8) investigated the ionic conductivity and density and compared it to the sintered material. It explained the difference in the ionic conductivity between the hot-pressed and sintered materials entirely on the difference in relative density between these two materials. No information was given on the microstructure (i.e., grain size) of the hot-pressed and sintered materials. This is important because it is well-known that hot-pressing and sintering cannot only have different relative densities, but also different grain sizes, which can cause a difference in behavior (12–14). Thus, it is important if hot-pressing is to be used as a consolidation method, as one must not only characterize the relative density but also the microstructure. At present such information is lacking for hot-pressed LTP. Furthermore, there is no information on mechanical properties of hot-pressed LTP. Again, such information is

needed if hot-pressing is to be used to produce dense membranes for use in Li-Air batteries, since mechanical properties like ionic conductivity are a strong function of the microstructure.

It is the purpose of this report to present the first detailed comparison of both the electrical and mechanical properties of hot-pressed versus sintered $\text{LiTi}_2(\text{PO}_4)_3$, and relate these properties to the microstructure.

2. Experimental

2.1 Powder Characterization

$\text{LiTi}_2(\text{PO}_4)_3$ powders were obtained from Ceramatec, Inc. (Salt Lake City, Utah). The structure of the as-received powders and the consolidated products was characterized by X-ray diffraction. Lattice constants were determined by obtaining diffraction data in a parallel beam diffraction geometry and fitting the data using Rietveld refinement (15). The LTP particle size distribution was determined using a Scanning Electron Microscope (SEM). The LTP specific surface area was measured using nitrogen gas adsorption (Brunauer-Emmett-Teller (BET)).

2.2 Consolidation

The LTP powders were consolidated by conventional sintering or hot-pressing. Differential Thermal Analysis (DTA) was performed on the powders by Orton Materials Testing and Research Center (Westerville, OH) to determine if there was any glass phase(s) present during the consolidation step. For sintering, the LTP powders were first uniaxially pressed into cylindrical specimens 13 mm in diameter with a thickness between 2–4 mm at a pressure of 200 MPa. A 5 wt. % polyvinyl alcohol binder was used. The pellets were then sintered at 1050 °C for 1 h under air on platinum foil. This temperature was chosen since it is in the typical range (900–1250 °C) used for sintering of pure and doped LTP (2–8,11). For hot-pressing, about 15 g of powder was placed in a graphite die lined with graphfoil, which was then heated to 1050 °C, at which time a stress of 40 MPa was applied and held for a period of 1 h. The load was then removed and sample cooled to room temperature. During the heating and cooling stages, the furnace was flushed with flowing argon. The hot-pressed specimen was disc-shaped with a thickness of about ~11 mm and a diameter between 22–23 mm. Rectangular parallelepiped specimens of about 5 mm × 5 mm × 3 mm were cut from the hot-pressed disc using a low-speed diamond saw for microstructural analysis, density, and electrical and mechanical property measurements.

2.3 Property Characterization

The bulk density of the sintered and hot-pressed samples was determined from the weight and physical dimensions, and also by the Archimedes method using methanol as the immersion fluid. The relative density values were determined by dividing the bulk density by the LTP theoretical

density. The microstructure of the sintered and hot-pressed samples was examined using a SEM on fracture surfaces.

AC and DC room temperature electrical conductivity measurements were performed on sintered and hot-pressed samples using the two probe method. Silver paste electrodes were applied to the top and bottom surfaces of the specimens. AC measurements were undertaken to determine ionic conductivity. AC impedance was measured using a Solatron 1260 Impedance Analyzer in the frequency range 1 to 10^6 Hz. DC measurements were undertaken to determine electronic conductivity. DC resistances were measured using a Keithly 6517A Electrometer/High Resistance Meter with a Model 8009 Resistivity Test Fixture capable of measuring volume resistivities as high as 10^{18} ohms-cm. Samples for DC electronic conductivity required equilibration times of about 12–18 h to ensure steady-state was achieved.

The mechanical properties of the sintered and hot-pressed LTP materials were evaluated from microhardness measurements. Microhardness was chosen to characterize the mechanical properties of the sintered and hot-pressed LTP materials for the following reasons: 1) hardness is related to strength and 2) the small volume of material and ease of specimen preparation and testing (16–17). The room temperature Vickers hardness of polished sintered and hot-pressed specimens was measured using a Zwick microhardness tester. The hardness was measured at a load of 29.4 N at an indentation time of 30 s.

3. Results and Discussion

3.1 Color

The sintered LTP disc was colored white like the original starting powders. The hot-pressed disc had a blue color on the surface, but was white-colored in the interior. The blue color would suggest that on the surface some of the titanium had reduced from Ti^{+4} to Ti^{+3} as a result of the carbon foil and reducing atmosphere. A discussion of this blue surface layer is detailed in section 3.9, which concerns the electronic conductivity of LTP after heat-treatment under a reducing atmosphere. The blue surface layer was removed by polishing. To standardize the hot-pressed disc and ensure that all the titanium was in the +4 state, the hot-pressed disc, after removing the blue surface layer, was heated at 900 °C for 2 h under air prior to microstructural analysis, density, conductivity, and hardness measurements.

3.2 Particle Size

Scanning electron microscopy results of the as-received LTP powders shown in figure 1, revealed that a majority (~80 vol. %) of the powders were 1 μm or less. The remaining (~20 vol. %) particles were in the range 1 to 5 μm . No particles with sizes greater than 5 μm were

observed. The powder surface area was $4.52 \text{ m}^2/\text{g}$ from the BET measurements, which gives an average particle size of $\sim 0.5 \text{ }\mu\text{m}$, assuming spherical particles (18).

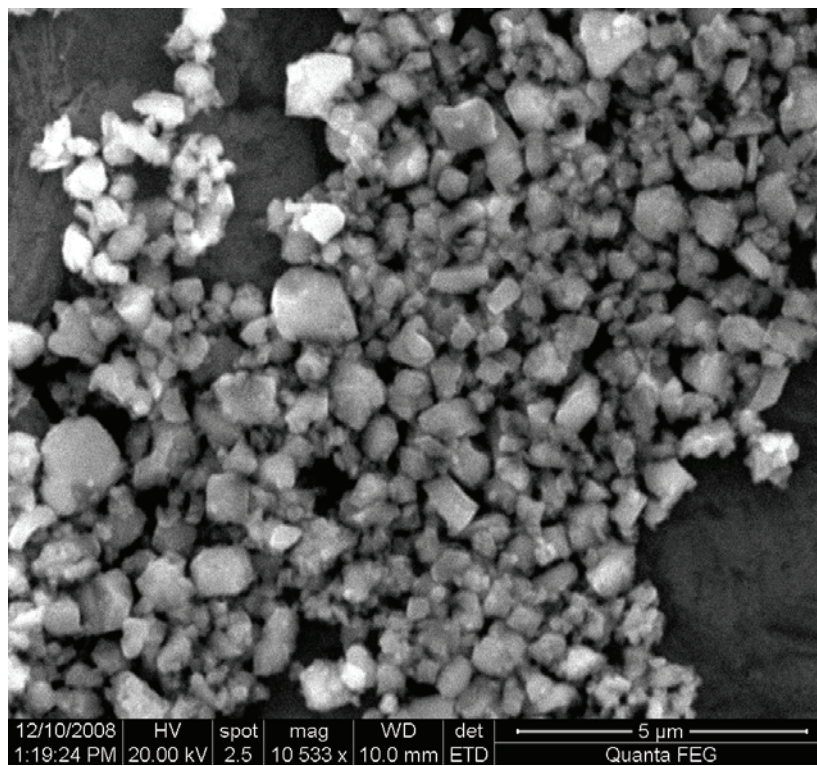


Figure 1. Scanning electron micrograph of the initial $\text{LiTi}_2(\text{PO}_4)_3$ powders.

3.3 Structure

The X-ray diffraction pattern for the as-received LTP powder is shown in figure 2a ($\text{Cu K}\alpha$ radiation). Figure 2a illustrates that the powder is almost pure single phase $\text{LiTi}_2(\text{PO}_4)_3$. Rietveld refinement suggested that the amount of second phase TiO_2 (rutile) shown by the star is less $< 1 \text{ wt. } \%$. TiO_2 has been observed in LTP samples as a result of Li_2O loss after calcining and/or sintering (19,20). All diffraction lines of LTP can be indexed based on a rhomboheral structure with a $R3c$ space group. The lattice parameters determined using Rietveld refinement yielded $a=8.5114 \text{ \AA}$ and $c=20.8408 \text{ \AA}$. These values are in good agreement with values listed in the literature (21). The X-ray diffraction patterns for LTP after sintering, after hot-pressing (blue surface layer was removed prior to grinding the powders for X-ray diffraction), and after hot-pressing and annealing are shown in figures 2b–d, respectively. A comparison of figures 2b–d with that for the starting powders (figure 2a) reveals that no new phases appeared and that there was no change in the position of the peaks. A comparison of the X-ray diffraction pattern for the hot-pressed powder (figure 2c) with the starting powder (figure 2a) and sintered powder (figure 2c) reveals that there is some change in the relative intensity of the peaks. This may be a result of some preferred alignment that takes during hot-pressing. After the annealing step (figure 2d), it is seen that much of the preferred alignment is reduced and the relative intensities of the peaks

are similar those for the as-received (figure 2a) and sintered (figure 2b) powders. The lattice parameters determined using Rietveld refinement yielded $a=8.5129 \text{ \AA}$ and $c=20.8502 \text{ \AA}$, and $a=8.5118 \text{ \AA}$ and $c=20.8529 \text{ \AA}$, respectively for the hot-pressed and annealed and the sintered materials. These are in good agreement with values for the as-received powders. The X-ray diffraction results suggest that both the sintered and hot-pressed and annealed materials have the same structure.

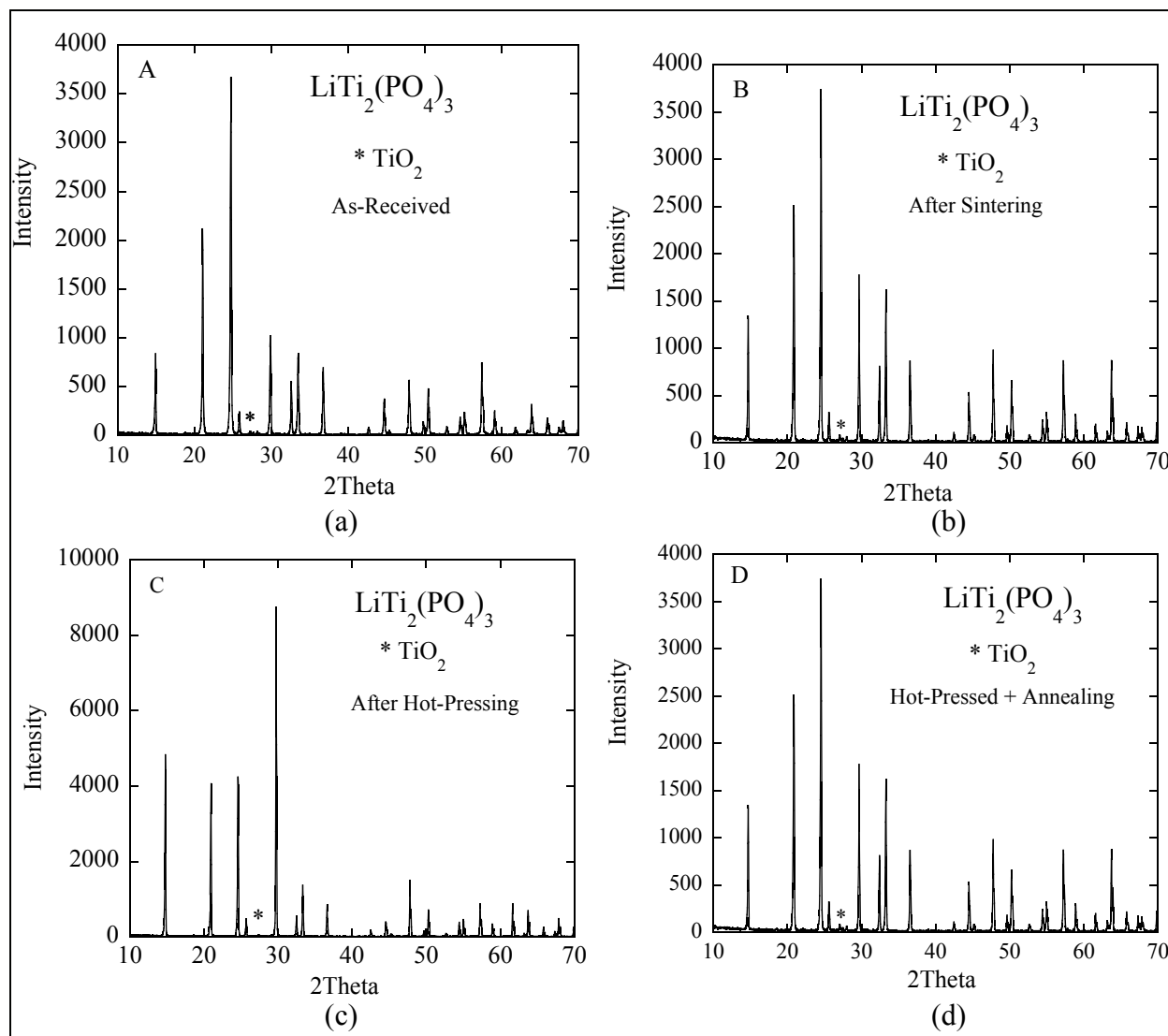


Figure 2. (a) X-ray diffraction pattern of the as-received $\text{LiTi}_2(\text{PO}_4)_3$ powders, (b) X-ray diffraction pattern of the $\text{LiTi}_2(\text{PO}_4)_3$ powders after sintering, (c) X-ray diffraction pattern of the $\text{LiTi}_2(\text{PO}_4)_3$ powders after hot-pressing, and (d) X-ray diffraction pattern of the $\text{LiTi}_2(\text{PO}_4)_3$ powders after hot-pressing and annealing.

3.4 Differential Thermal Analysis

The DTA curve for the LTP powders heated at $10 \text{ }^\circ\text{C}/\text{min}$ from room temperature to $1400 \text{ }^\circ\text{C}$ under air is shown in figure 3. From figure 3 it can be seen that there are no sharp endothermic peaks at the sintering/hot-pressing temperature of $1050 \text{ }^\circ\text{C}$, suggesting that during the

consolidation step we should have only solid state sintering (i.e., no liquid phase sintering). The gradual endothermic slope in the curve at high temperature is associated with Li_2O loss (8,11).

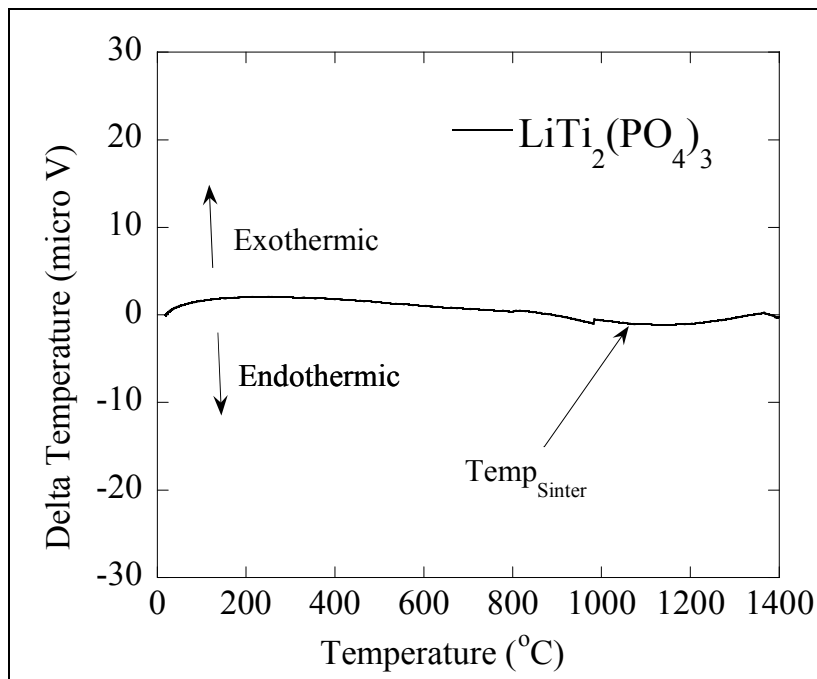


Figure 3. Differential thermal analysis curve (heating) for $\text{LiTi}_2(\text{PO}_4)_3$ powders.

3.5 Density

The relative density of the sintered and hot-pressed and annealed LTP samples is $82\pm 2\%$ and $88\pm 2\%$, respectively (theoretical density = 2.948 g/cm^3 [21]). The values based on the physical dimensions and weight are in close agreement with those determined using the Archimedes method. The relative density of sintered LTP ($82\pm 2\%$) is in agreement with the value of $\sim 77\%$ obtained by Ando, et al. (8) on LTP powders sintered at the same temperature ($1050 \text{ }^\circ\text{C}$; the sintering time was not specified). The relative density of the present sintered LTP is higher than that reported by Wolfenstine, et al. (11) of about 69% for LTP sintered at $950 \text{ }^\circ\text{C}$ for 2 h, and Aono, et al. (6) of about 67% for LTP sintered between $900\text{--}1250 \text{ }^\circ\text{C}$ (the exact sintering temperature was not specified (6)). The differences in densities between these studies and the present could be a result of several factors including different temperatures, times, heating rates, starting particle size, packing, and impurity content (12–14). The higher density of the hot-pressed sample compared to the sintered sample is expected, since the addition of the applied stress during hot-pressing increases the driving force for densification over that for conventional sintering (12–14). The results of the present study are in agreement with results of Ando, et al. (8), who observed a higher density for hot-pressed LTP ($\sim 95\%$) versus sintered LTP ($\sim 83\%$) heated at $1100 \text{ }^\circ\text{C}$, and the recent results of Zhu, et al. (22) on NASICON ($\text{Na}_3\text{Zr}_2\text{Si}_2\text{PO}_{12}$), who observed that NASICON hot-pressed under a stress of 20 MPa at $1000 \text{ }^\circ\text{C}$ also exhibited a higher density ($\sim 94\%$) compared to the same material sintered at $1000 \text{ }^\circ\text{C}$ ($\sim 83\%$).

3.6 Microstructure

Fracture surfaces of the sintered, hot-pressed, and annealed LTP samples are shown in figures 4, 5, and 6, respectively. Several important points are also noted. Firstly, both the sintered and hot-pressed microstructures reveal a duplex microstructure composed of fine grains ($<5\ \mu\text{m}$) and large grains ($>20\ \mu\text{m}$). Secondly, the percentage of fine grains is much higher in the sintered material than in the hot-pressed material, leading to a large average grain size for the hot-pressed material compared to the sintered material. The results reveal that a significant amount of growth grain has occurred during both sintering and hot-pressing, since the average starting grain size was $\sim 0.5\ \mu\text{m}$ (figure 1). Grain growth is to be expected in pure LTP since it is a single phase material (figure 1) with no intentionally added second phases (the amount of residual TiO_2 is very small) or solute impurities to pin down grain boundaries (12–14,23–26). What is unusual about the grain growth of both materials is that it is very abnormal/discontinuous (i.e., rapid growth of a few grains), leading to a duplex microstructure. At present it is not clear what has caused the abnormal/discontinuous grain growth of the sintered and hot-pressed materials. Abnormal/discontinuous grain growth can result from nonuniformities in impurity content, inhomogeneous packing of the starting powders, anisotropies in grain boundary energy, and mobility and the presence of a liquid phase along the grain boundaries (13,14). In most materials abnormal/discontinuous grain growth is associated with the presence of a liquid phase along the grain boundaries (12–14,27–29). This can be most likely ruled out for our case because the DTA results (figure 3) revealed no liquid phase (no sharp endothermic peak) at the sintering/hot-pressing temperature. However, to conclusively rule out this possibility would require one to heat a sample to the sintering/hot-pressing temperature, quench it to room temperature, and then do detailed transmission electron microscopy on it. To determine the exact reason for the abnormal/discontinuous grain growth would require a detailed study, which is beyond the scope of the present investigation.

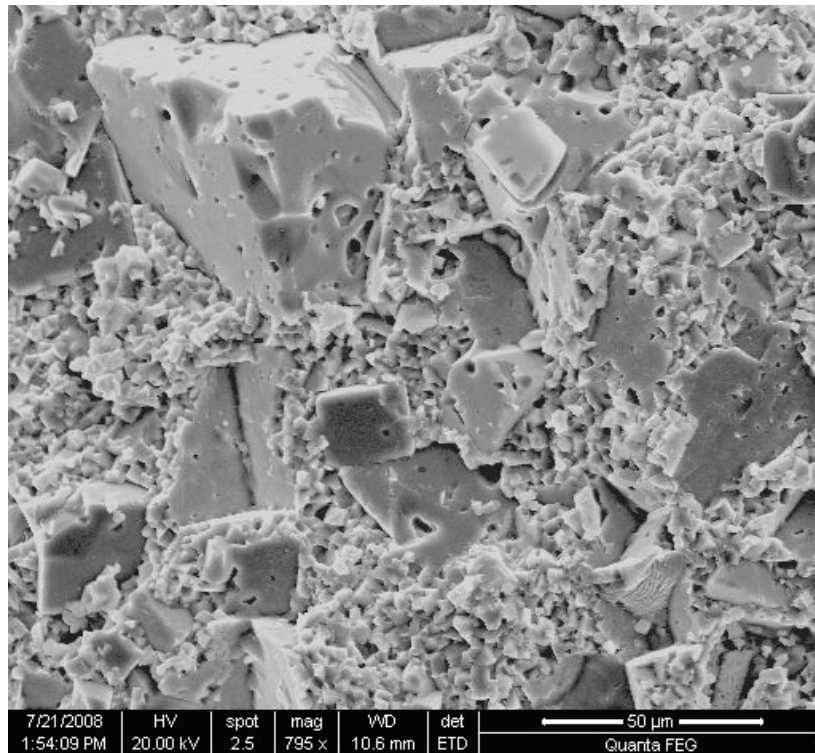


Figure 4. Scanning electron micrograph of sintered $\text{LiTi}_2(\text{PO}_4)_3$ fracture surface.

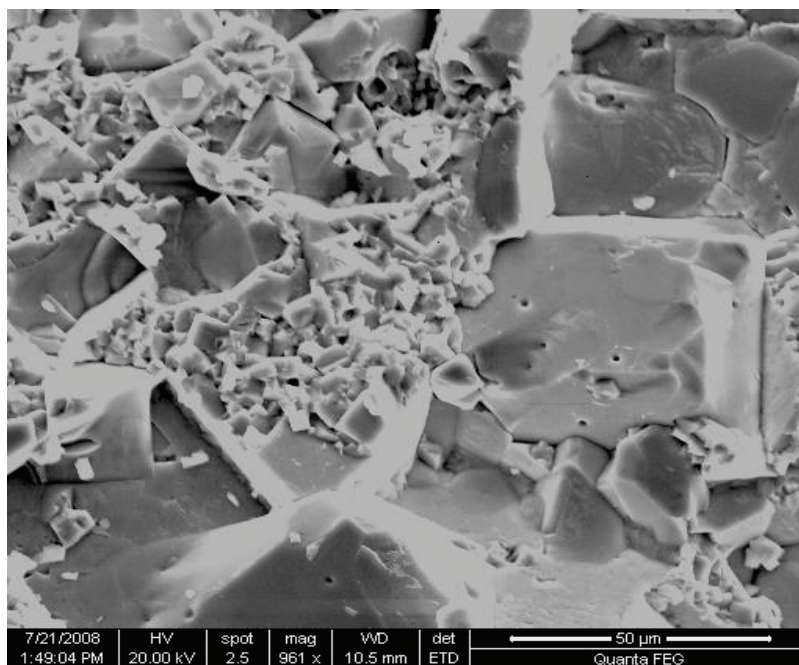


Figure 5. Scanning electron micrograph of hot-pressed $\text{LiTi}_2(\text{PO}_4)_3$ fracture surface.

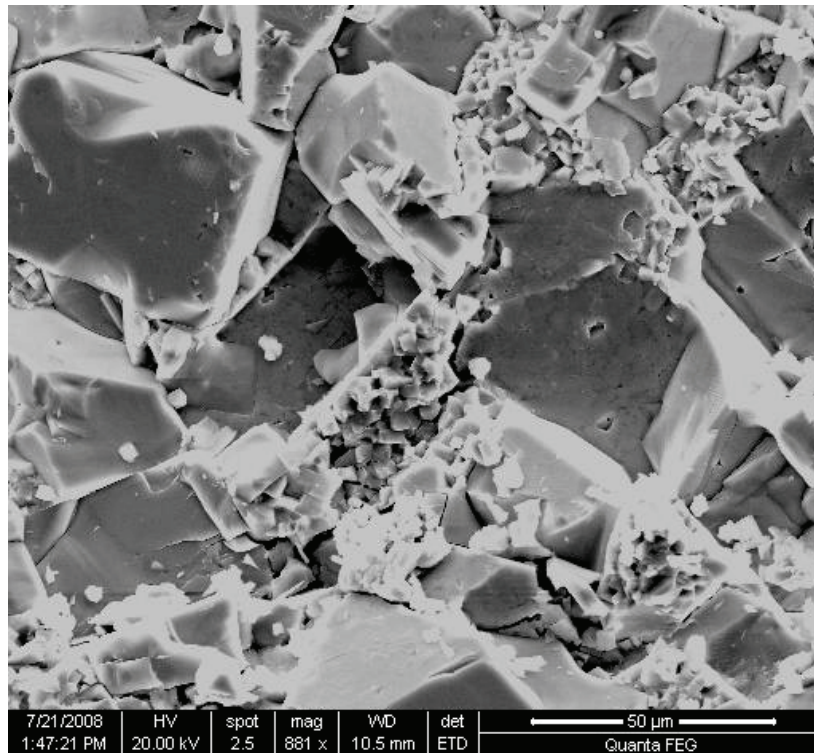


Figure 6. Scanning electron micrograph of hot-pressed and annealed $\text{LiTi}_2(\text{PO}_4)_3$ fracture surface.

One possible reason for the difference in microstructure between the sintered and hot-pressed materials—the larger average grain size of the hot-pressed sample compared to the sintered sample—is a result of the extra annealing step (900 °C for 2 h) given to the hot-pressed sample. A comparison of the microstructure of the as-hot pressed (figure 5) to the hot-pressed and annealed (figure 6) material revealed no change in microstructure had occurred as a result of the annealing step. Hence, the annealing step cannot explain the difference in microstructure. Likely reasons for the larger average grain size of the hot-pressed material compared to the sintered material are a result of the applied stress and higher density. It has been observed that materials, when heated at high temperature under load, exhibit a larger grain size, known as dynamic grain growth, than the same material when heated at the same high temperature with no load, known as static grain growth, as a result of stress enhanced diffusion (30–34). A higher density leads to a lower number of pores along boundaries, which reduces the drag force on the boundaries and hence, promotes grain growth (12–14,23–26).

3.7 Electronic Conductivity

The electronic conductivities of the sintered and hot-pressed and annealed sample is 1×10^{-9} S/cm and 2×10^{-9} S/cm, respectively. These values are in excellent agreement with each other. This is expected since the sintered and hot-pressed powders come from the same source (i.e., have the same background impurities) and had nearly the same heat-treatment (one sintered

under air and the other annealed under air). These values are in agreement with the electronic conductivity value of less than 10^{-9} S/cm for LTP consolidated by spark-plasma sintering (20).

3.8 Ionic Conductivity

The room temperature AC conductivity results for the sintered LTP and hot-pressed and annealed LTP samples using Li-ion blocking silver electrodes are shown in the full complex impedance plot in figure 7. From figure 7, several important points are observed. Firstly, the data for both samples separates into a high frequency region which contains a semicircle and low frequency region which contains a spike. For this case, since we have Li blocking electrodes, the shape of the curve represents a material which is predominately a Li-ion conductor with very low electronic conductivity (35–38). Secondly, the low frequency intercept of the semicircle on the Z' axis gives the total ionic resistance, which includes the contribution of the lattice and the grain boundary components (5,10,37,38). Using this resistance and sample dimensions, the total ionic conductivity of the sintered and hot-pressed LTP samples was calculated. The total ionic conductivity of the sintered sample is 4×10^{-8} S/cm whereas, for the hot-pressed and annealed sample, the total ionic conductivity is 2×10^{-7} S/cm. The total ionic conductivity of the hot-pressed and annealed sample is about five times higher than that for the sintered sample. These results are in agreement with the recent hot-pressed versus sintered NASICON results of Zhu, et al. (22), who observed about a factor of 2 increase in total ionic conductivity for the hot-pressed material compared to the sintered material and the results of Ando, et al. (8) for LTP, who observed an increase of about a factor of 8 for the hot-pressed material compared to the sintered material.

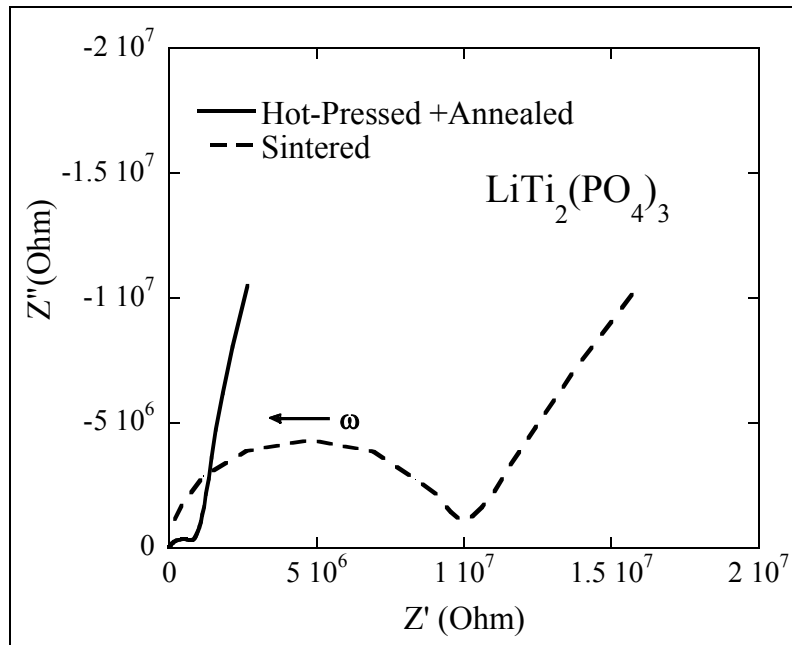


Figure 7. Complex impedance plot of sintered and hot-pressed and annealed $\text{LiTi}_2(\text{PO}_4)_3$.

A blow-up of the high frequency end of the semi-circle shown in figure 7 is shown in figure 8. A second semicircle is typically observed between the origin and the intercept on the Z' axis (36–38). This semicircle would be observed if higher frequencies were used (36,39). The intercept of the line on the Z' axis gives the Li-ion lattice conductivity (35–39). Using this resistance and sample dimensions, the lattice conductivity of the sintered and hot-pressed and annealed LTP samples was calculated. From figure 8 it is observed that the data for both the sintered and hot-pressed and annealed LTP samples superimposes onto one curve, yielding the same value of lattice conductivity. This is expected since the sintered and hot-pressed powders come from the same source (i.e., have the same background impurities) and had nearly the same heat-treatment (one sintered under air and the other annealed under air). The value of the Li-ion lattice conductivity for both samples is $\sim 6 \times 10^{-4}$ S/cm. This value of the Li-ion lattice conductivity is in good agreement with the Li-ion lattice conductivity of LTP and Al-doped LTP materials (2–11). A comparison of the lattice conductivity ($\sim 6 \times 10^{-4}$ S/cm) with the total conductivity, lattice plus grain boundary (4×10^{-8} S/cm for the sintered material 2×10^{-7} S/cm for the hot-pressed and annealed material), confirms what has been suggested in the literature (2–11), in that the ionic conductivity of polycrystalline LTP materials is controlled by the higher resistivity grain boundaries. Furthermore, since the lattice conductivity of the both the hot-pressed and annealed and sintered material is the same, the higher total conductivity of the 2×10^{-7} S/cm for the hot-pressed and annealed material compared 4×10^{-8} S/cm must be due to a difference in the resistance of the grain boundary component between these two materials.

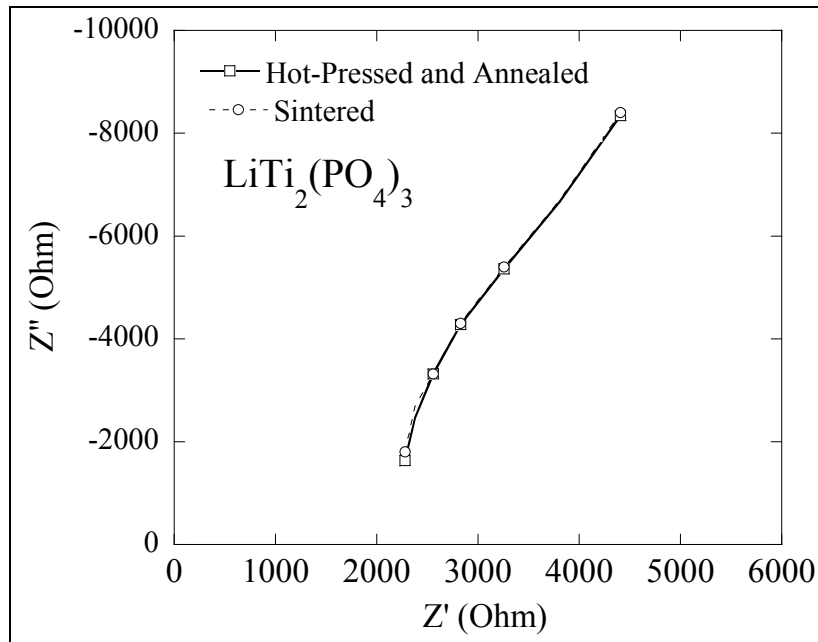


Figure 8. High frequency region of the complex impedance plot of sintered and hot-pressed and annealed $\text{LiTi}_2(\text{PO}_4)_3$.

The difference in the ionic conductivity of the grain boundary component of the hot-pressed and annealed LTP material compared to the sintered LTP material is a result of two factors. The first

factor is the higher density of the hot-pressed material (~88%) versus the sintered material (~82%). It has been observed that as the density increases, the total ionic conductivity increases as a result of the decrease in the resistance component associated with grain boundaries (2,4–6,10,39,40). The second factor is a result of the difference in microstructure for the two materials. From figures 4 and 6 it can be observed that the hot-pressed and annealed material has a larger average grain size than for the sintered material. It has been shown that as the grain size increases, the total ionic conductivity increases as a result of the decrease in the resistance component associated with grain boundaries decreases (4,5,41–43). Consequently, as a result of the higher density and larger average grain size of the hot-pressed LTP material, the resistance component associated with grain boundaries is lower for this material compared to the sintered LTP material, and hence, a higher total ionic conductivity is exhibited by the hot-pressed LTP material.

The ionic transport number (ionic conductivity/total conductivity) for hot-pressed LTP is ~0.99 and for sintered LTP is ~0.97. These results confirm that LTP, when heated under oxidizing conditions, is an ionic conductor.

3.9 Electronic Conductivity Under Reducing Atmosphere

It was observed that when both the hot-pressed and annealed and sintered materials were heated under a reducing atmosphere (3 vol.% H₂-balance Ar) at 800 °C for 12 h, they both had a bluish color. It is believed that this color change is associated with a change in some of the Ti⁺⁴ ions being reduced to Ti⁺³ ions according to equation 1 with charge neutrality given by equation 2 (12–14).



Where O_o^x represents an oxygen ion and V_o^{••} represents an oxygen vacancy, an electron, e', corresponds to Ti⁺³ on a Ti⁺⁴ site [Kroger-Vink (12–14) notation is used]. It has been shown in Li₄Ti₅O₁₂ (44,45), which is colored white after heating in a oxidizing atmosphere, that after heat-treatment in a reducing atmosphere it was blue colored, as a result of some Ti⁺⁴ ions being reduced to Ti⁺³ ions. X-ray photoelectron spectroscopy confirmed the formation that the color change from white to blue for Li₄Ti₅O₁₂ resulted from some of the Ti⁺⁴ ions having been reduced to Ti⁺³ ions during heat-treatment under reducing conditions (44). In addition, it has been shown in TiO₂ by X-ray photoelectron spectroscopy (XPS) that heating under a reducing atmosphere caused some of the Ti⁺⁴ ions to transform to Ti⁺³ ions (46). Also in TiO₂, samples heated under low oxygen partial pressure have shown that electron paramagnetic resonance revealed the presence of Ti⁺³ centers where none were observed for samples heated in air (47). Since the main species capable of changing oxidation state in LTP is Ti, similar to that for the case of Li₄Ti₅O₁₂ and TiO₂, it is highly likely that the blue color of LTP heated in a reducing atmosphere is also a result of some of the Ti⁺⁴ ions having been reduced to Ti⁺³ ions. Further proof of the

existence of Ti^{+3} in the reduced samples will be given in the next paragraph on the X-ray diffraction patterns for LTP heated under a reducing atmosphere.

The X-ray diffraction of the sintered and hot-pressed and annealed LTP powders heated under a reducing atmosphere is shown in figures 9 and 10, respectively. A comparison of these figures with each other and figure 2 reveals that the patterns for LTP heated under air or H_2/Ar are similar. Lattice constants were determined by obtaining diffraction data in a parallel beam diffraction, geometry revealed that the only difference was a slight shift in the diffraction peaks to the lower 2θ values for the samples heated under H_2/Ar compared to under air. The lattice parameter of the H_2/Ar hot-pressed and annealed LTP sample determined from Rietveld analysis of the XRD pattern yielded $a=8.6514 \text{ \AA}$ and $c=20.9708 \text{ \AA}$, and the sintered LTP sample under a reducing atmosphere yielded $a=8.6598 \text{ \AA}$ and $c=21.0003 \text{ \AA}$. The lattice parameters of the H_2/Ar samples are larger compared to the air samples (section 3.3). This result is expected if some of the Ti^{+4} transformed to Ti^{+3} , because of the larger size of the Ti^{+3} ion (0.81 \AA) compared to the Ti^{+4} ion (0.75 \AA) (12).

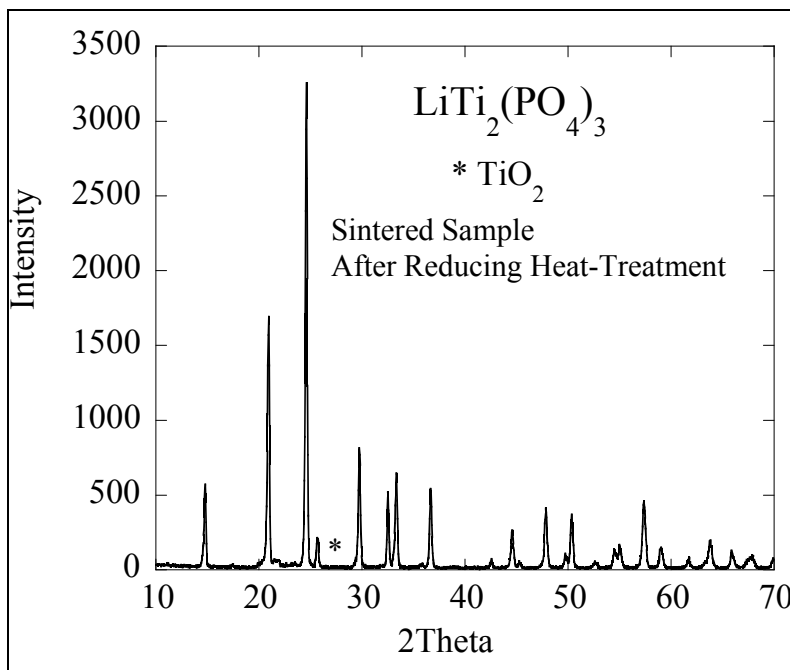


Figure 9. X-ray diffraction pattern of the $\text{LiTi}_2(\text{PO}_4)_3$ sintered sample after heating under a reducing atmosphere.

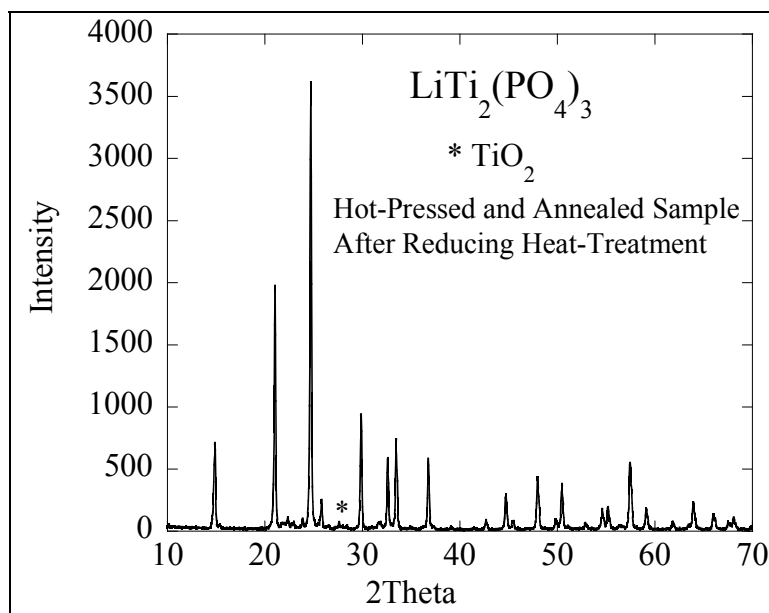


Figure 10. X-ray diffraction pattern of the $\text{LiTi}_2(\text{PO}_4)_3$ hot-pressed and annealed sample after heating under a reducing atmosphere.

DC electronic values of 8×10^{-3} S/cm and 9×10^{-3} S/cm were exhibited by the sintered and hot-pressed and annealed materials, respectively, after heat-treatment under the reducing atmosphere. The values are in excellent agreement with each other. These values ($\sim 10^{-2}$ S/cm) are about a factor of $10^7 \times$ higher than that for the same materials when heated under air ($\sim 10^{-9}$ S/cm). The electronic conductivity after heating in a reducing atmosphere of about 10^{-2} S/cm for both materials suggests that they are predominately electronic conductors, as a result of the transition of some Ti^{+4} to Ti^{+3} , which increases the number of electrons and, hence, electronic conductivity (45,48).

Increasing the electronic conductivity of LTP is important if it is to be used as an electrode in Li-ion batteries. For example, LTP has been investigated as a possible anode for use in Li-ion batteries (47,48). It was observed that one of the problems with an LTP anode heat-treated in air was its low rate capability, which is a result of its low electronic conductivity (49,50). The above procedure (i.e., heating LTP under a reducing atmosphere) demonstrates a method to increase the electronic conductivity of LTP to $\sim 10^{-2}$ S/cm, about 10^7 times greater than that for heat-treatment under air, and within the electronic conductivity range of typical oxide cathodes used in Li-ion batteries ($\text{LiCoO}_2 \sim 10^{-3}$ S/cm (51) and $\text{LiMn}_2\text{O}_4 \sim 10^{-5} - 10^{-4}$ S/cm (52)). It is, therefore, expected that LTP heated under a reducing atmosphere as result of its higher electronic conductivity will exhibit a higher rate capability than when heated under an air atmosphere.

3.10 Microhardness

The hardness of sintered LTP was ~ 92 HV. This is about twice that for the hot-pressed and annealed LTP (~ 50 HV), which implies a higher strength for the sintered material. There are two

major microstructural features that influence the hardness/strength of these materials. The first is porosity. Pores reduce the strength of a material by reducing the cross-sectional over which the load is applied and acting as stress concentrators (12,14). If this were the only factor, it would be expected that the hot-pressed and annealed material with its lower porosity (i.e., higher density) versus the sintered material should have the higher hardness/strength. This is opposite to the experimental results, where a higher hardness was observed for the sintered material, the one with the lowest density. The second factor is grain size (12,52–55). It is known that as grain size increases, hardness/strength decreases. Typically it is observed that hardness/strength varies inversely with grain size to the one-half power (52–55). The explanation for this effect is that in this regime the flaw size scales with grain size (12,52–55). From figures 3 and 4 it can be observed that the hot-pressed material has a larger average grain size than for the sintered material, hence, based on the grain size effect, the hot-pressed and annealed material with the larger grain size should exhibit a lower hardness/strength than the sintered material. This prediction is in agreement with the experimental results. Consequently, the results suggest that of the two microstructural variables investigated in this study, grain size and porosity, the one that dominates the hardness/strength of the two LTP materials is grain size.

4. Conclusions

The electrical and mechanical properties of hot-pressed (40 MPa, 1050 °C, 1 h) versus sintered (1050 °C, 1 h) $\text{LiTi}_2(\text{PO}_4)_3$ was investigated. The hot-pressed $\text{LiTi}_2(\text{PO}_4)_3$ had a higher density and larger average grain size than the sintered material. As a result of these microstructural differences, the hot-pressed material exhibited a higher total ionic conductivity and lower hardness. The electronic conductivity of the sintered and hot-pressed and annealed sample when heated under air is about the same, $\sim 1 \times 10^{-9}$ S/cm, which increased to $\sim 10^{-2}$ S/cm, when both were heated under a reducing atmosphere. This increase in electronic conductivity is a result of the transition of some Ti^{+4} to Ti^{+3} , which increases the number of electrons. The results of this study reveal that ionic conductivity and hardness of $\text{LiTi}_2(\text{PO}_4)_3$ are a strong function of the microstructure. In order to obtain dense $\text{LiTi}_2(\text{PO}_4)_3$ with optimized properties for use in Li-Air batteries, the consolidation conditions must be carefully chosen.

5. References

1. Visco, S. J.; Katz, B. D.; Nimon, Y. S.; De Jonghe, L. C. U.S. Pat. 7,282,295 B2, 2007.
2. Adachi, G.; Imanaka, N.; Aono, H. *Adv. Mater.* **1996**, 8, 127
3. Aono, H.; Sugimoto, E.; Sadaoka, Y.; Imanaka, N.; Adachi, G. *Solid State Ionics* **1990**, 38, 40–41.
4. Aono, H.; Sugimoto, E.; Sadaoka, Y.; Imanaka, N.; Adachi, G. *Solid State Ionics* **1991**, 47, 257.
5. Aono, H.; Sugimoto, E.; Sadaoka, Y.; Imanaka, N.; Adachi, G. *J. Electrochem. Soc.* **1993**, 140, 1827.
6. Aono, H.; Sugimoto, E.; Sadaoka, Y.; Imanaka, N.; Adachi, G. *J. Electrochem. Soc.* **1990**, 137, 1023.
7. Aono, H.; Sugimoto, E.; Sadaoka, Y.; Imanaka, N.; Adachi, G. *Chem Lett.* **1990**, 1825.
8. Ando, Y.; Hirose, N.; Kuwano, J.; Kato, M.; Otsuka H. in: P. Vincenzini (Ed.), *Ceramics Today-Tomorrow's Ceramics*, Elsevier Science Publ., Amsterdam, 1991, p. 2245.
9. Fu, J. U.S. Pat. 6,485,622 B1, 2002.
10. Fu, J. *Solid State Ionics* **1997**, 96, 195.
11. Wolfenstine, J.; Foster, D.; Read, J.; Allen, J. L. *J. Power Sources* **2008**, 182, 626.
12. Barsum, M. V. *Fundamentals of Ceramics*; The McGraw-Hill Companies, Inc. New York, 1997.
13. Chiang, Y. M.; Birnie III, D.; Kingery, W. D. *Physical Ceramics*; Wiley: New York, 1997.
14. Kingery, W. D.; Bowen, H. K.; Uhlmann, D. R. *Introduction to Ceramics*; (second ed), Wiley: New York, 1976.
15. Rietveld, H. M. *J. Appl. Crystall.* **1969**, 2, 65.
16. Ashby, M. F.; Jones, D.R.H. *Engineering Materials: An Introduction to their Properties and Applications*; Pergamon Press, Oxford, 1980.
17. Richerson, D. W. *Modern Ceramic Engineering: Properties, Processing, and Use in Design* (second ed), Marcel Dekker, Inc., New York, 1992.
18. Kavan, L.; Gratzel, M. *Electrochem. Solid-State Lett.* **2002**, 5, A39.

19. Wong, S.; Newman, P.; Best, J.A.S.; Nairn, K. M.; MacFarlane, D.; Forsyth, R. M. *J. Mater. Chem.* **1998**, *8*, 2199.
20. Kobayashi, Y.; Takeuchi, T.; Tabuchi, M.; Ado, K.; Kageyama, H. *J. Power Sources* **1999**, *853*, 81–82.
21. Joint Commission on Powder Diffraction Standards (JCPDS) PDF#:00-035-0754, International Center for Diffraction Data, Newton Square, PA USA.
22. Zhu, D.; Luo, F.; Xie, A.; Zhou, W. *Rare Metals* **2006**, *25*, 39.
23. Bennison, S. J.; Harmer, M. P. *J. Am. Ceram. Soc.* **1985**, *68*, C-22.
24. Bennison, S. J.; Harmer, M. P. *J. Am. Ceram. Soc.* **1983**, *66*, C-90.
25. Brooke, R. J. *Scr. Metall.* **1968**, *2*, 355.
26. Cahn, J. W. *Acta Metall.* **1962**, *10*, 789.
27. Bateman, C. A.; Bennison, S. J.; Harmer, M. J. *J. Am. Ceram. Soc.* **1989**, *72*, 1241.
28. Kaysser, W. A.; Sprissler, M.; Handwerker, C. A.; Blendell, J. E. *J. Am. Ceram. Soc.* **1987**, *70*, 339.
29. Shi, D.; Capone II, D. W.; Goudey, G. T.; Singh, J. P.; Zaluzec, N. J.; Goretta, K. J. *Mat. Lett.* **1988**, *6*, 217.
30. Nieh, T.-G.; Wadsworth, J. *J. Am. Ceram. Soc.* **1989**, *72*, 1469.
31. Carry, C.; Mocellin, A. *Ceram. Inter.* **1987**, *13*, 89.
32. Fridez, C. D.; Carry, C.; Mocellin, A. in *Advances in Ceramics Vol. 10, Structure and Property of MgO and Al₂O₃ Ceramics*. ed. W.D. Kingery (American Ceramic Society, Columbus, OH, 1984) p. 720.
33. Xue, L. A.; Chen, I.-W. *J. Am. Ceram. Soc.* **1990**, *73*, 3518.
34. Ventkatachari, K. R.; Raj, R. *J. Am. Ceram. Soc.* **1986**, *69*, 135.
35. Jamnik, J.; Maier, J. *J. Electrochem. Soc.* **1999**, *146*, 4183.
36. Chen, C. H.; Amine, K. *Solid State Ionics* **2001**, *144*, 51.
37. Huggins, R. A. *Ionics* **2002**, *8*, 300.
38. Baurle, J. E. *J. Phys. Chem Solids* **1969**, *30*, 2657.
39. Birke, P.; Salam, F.; Doring, S.; Weppner, W. *Solid State Ionics* **1999**, *118*, 149.
40. Aono, H.; Sugimoto, E.; Sadaoka, Y.; Imanaka, N.; Adachi, G. *Chem Lett.* **1990**, 331.

41. Fuentes, R. O.; Figueiredo, F. M.; Marques, F.M.B.; Franco, J. I. *Solid State Ionics* **2001**, *140*, 173.
42. Kim, J.-G.; Kim, H. G.; Chung, H.-T. *J. Mater. Sci. Lett.* **1999**, *18*, 493.
43. Ban, C. W.; Choi, G. M. *Solid State Ionics* **2001**, *140*, 285.
44. Wolfenstine, J.; Lee, U.; Allen, J. L. *J. Power Sources* **2006**, *154*, 287.
45. Wolfenstine, J.; Allen, J. L. *J. Power Sources* **2008**, *180*, 582.
46. Wang, R.; Hasimoto, K.; Fujishima, A.; Chikuni, M.; Kojima, E.; Kitamura, A.; Shimohigoshi, M.; Watanbe, T. *Adv. Mater.* **1998**, *10*, 135.
47. Konstantinova, E.; Weidmann, J.; Dittrich, Th. *J. Porous Mater.* **2000**, *7*, 389.
48. Yan, M. F.; Rhodes, W. W. *Appl. Phys. Lett.* **1982**, *40*, 536.
49. Delmas, C.; Nadiri, A.; Soubeyroux, J. L. *Solid State Ionics* **1988**, *419*, 28–30.
50. Wang, G. X.; Bradhurst, D. H.; Dou, S. X.; Liu, H. K. *J. Power Sources* **2003**, *124*, 231.
51. Molenda, J.; Stoklosa, A.; Bak, T. *Solid State Ionics* **1989**, *36*, 53.
52. Shimakawas, Y.; Numata, Y.; Tabuchi, J. *J. Solid State Chem.* **1997**, *131*, 138.
53. Carnigila, S. C. *J. Am. Ceram. Soc.* **1965**, *48*, 581.
54. Virkar, A. V.; Gordon, R. S. *J. Am. Ceram. Soc.* **1977**, *60*, 58.
55. Singh, J. P.; Virkar, A. V.; Shetty, D. K.; Gordon, R. S. *J. Am. Ceram. Soc.* **1979**, *62*, 179.

NO. OF COPIES	ORGANIZATION	NO. OF COPIES	ORGANIZATION
1 PDF	ADMNSTR DEFNS TECHL INFO CTR ATTN DTIC OCP 8725 JOHN J KINGMAN RD STE 0944 FT BELVOIR VA 22060-6218	1	US ARMY RSRCH LAB ATTN AMSRD ARL CI OK TP TECHL LIB T LANDFRIED BLDG 4600 ABERDEEN PROVING GROUND MD 21005-5066
1	DARPA ATTN IXO S WELBY 3701 N FAIRFAX DR ARLINGTON VA 22203-1714	1	DIRECTOR US ARMY RSRCH LAB ATTN AMSRD ARL RO EV W D BACH PO BOX 12211 RESEARCH TRIANGLE PARK NC 27709
1 CD	OFC OF THE SECY OF DEFNS ATTN ODDRE (R&AT) THE PENTAGON WASHINGTON DC 20301-3080	6	US ARMY RSRCH LAB ATTN AMSRD ARL CI OK PE TECHL PUB ATTN AMSRD ARL CI OK TL TECHL LIB ATTN AMSRD ARL SE DE J ALLEN ATTN AMSRD ARL SE DE J WOLFENSTINE ATTN AMSRD ARL SE EO J SUMNER ATTN IMNE ALC HR MAIL & RECORDS MGMT ADELPHI MD 20783-1197
1	US ARMY RSRCH DEV AND ENGRG CMND ARMAMENT RSRCH DEV AND ENGRG CTR ARMAMENT ENGRG AND TECHN LGY CTR ATTN AMSRD AAR AEF T J MATTS BLDG 305 ABERDEEN PROVING GROUND MD 21005-5001		
1	PM TIMS, PROFILER (MMS-P) AN/TMQ-52 ATTN B GRIFFIES BUILDING 563 FT MONMOUTH NJ 07703		
1	US ARMY INFO SYS ENGRG CMND ATTN AMSEL IE TD F JENIA FT HUACHUCA AZ 85613-5300		
1	COMMANDER US ARMY RDECOM ATTN AMSRD AMR W C MCCORKLE 5400 FOWLER RD REDSTONE ARSENAL AL 35898-5000		
1	US GOVERNMENT PRINT OFF DEPOSITORY RECEIVING SECTION ATTN MAIL STOP IDAD J TATE 732 NORTH CAPITOL ST NW WASHINGTON DC 20402		

INTENTIONALLY LEFT BLANK.